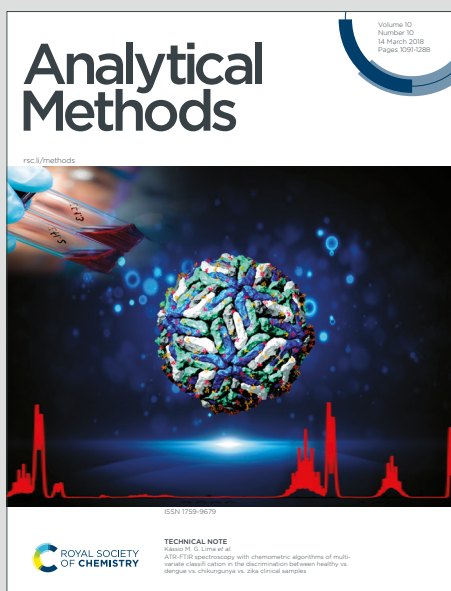


# Analytical Methods

Accepted Manuscript

This article can be cited before page numbers have been issued, to do this please use: S. Banerjee, Sk. A. Amin, S. Gayen, S. Priya, Y. Tomar, R. Taliyan and G. Singhvi, *Anal. Methods*, 2026, DOI: 10.1039/D5AY01534K.



This is an Accepted Manuscript, which has been through the Royal Society of Chemistry peer review process and has been accepted for publication.

Accepted Manuscripts are published online shortly after acceptance, before technical editing, formatting and proof reading. Using this free service, authors can make their results available to the community, in citable form, before we publish the edited article. We will replace this Accepted Manuscript with the edited and formatted Advance Article as soon as it is available.

You can find more information about Accepted Manuscripts in the [Information for Authors](#).

Please note that technical editing may introduce minor changes to the text and/or graphics, which may alter content. The journal's standard [Terms & Conditions](#) and the [Ethical guidelines](#) still apply. In no event shall the Royal Society of Chemistry be held responsible for any errors or omissions in this Accepted Manuscript or any consequences arising from the use of any information it contains.

# A Multimodal Approach Integrating Spectroscopy, Deep Learning guided Molecular Docking, and Molecular Dynamics simulation for predictive assessment of Pioglitazone to albumin binding for Formulation development

Saswata Banerjee<sup>1</sup>, Sk. Abdul Amin<sup>2</sup>, Shovanlal Gayen<sup>3</sup>, Sakshi Priya<sup>1</sup>, Yashika Tomar<sup>1</sup>,  
Rajeev Taliyan<sup>1</sup>, Gautam Singhvi<sup>1,\*</sup>

<sup>1</sup>Industrial Research Laboratory, Department of Pharmacy, Birla Institute of Technology and Science, Pilani, Pilani Campus, Vidya Vihar, Pilani, Rajasthan 333031, India.

<sup>2</sup>Department of Pharmacy, University of Salerno, Via Giovanni Paolo II, 132, 84084 Fisciano, SA, Italy.

<sup>3</sup>Laboratory of Drug Design and Discovery, Department of Pharmaceutical Technology, Jadavpur University, Kolkata, West Bengal 700032, India.

\*Corresponding Author: Dr. Gautam Singhvi, Industrial Research Laboratory, Department of Pharmacy, Birla Institute of Technology and Science, Pilani, Pilani Campus, Vidya Vihar, Pilani, Rajasthan 333031, India. Email: [gautam.singhvi@pilani.bits-pilani.ac.in](mailto:gautam.singhvi@pilani.bits-pilani.ac.in); Contact: 01596-255810

## Abstract

Binding affinity is a critical parameter that can influence the state of the drug in vivo and help to define the formulation strategy. The current study implements a multimodal approach to analyse the binding affinity between Human serum albumin (HSA) and Pioglitazone. Ultraviolet (UV) absorbance and Fluorescence spectrometry analysis were performed on different combinations of human serum albumin and Pioglitazone complexes, and the absorbance and fluorescence intensities were mapped to calculate the binding constant. DynamicBind, a distinct deep-learning artificial intelligence tool, was implemented to perform in-silico docking studies using a non-conventional approach. Further, molecular dynamics simulation was also performed to generate Root Mean Square Deviation, Radius of gyration, and Root Mean Square Fluctuation values, followed by Principal Component Analysis, Probability Distribution Function, and Free Energy Landscape analysis. The simulation output was analysed to interpret the binding affinity and associated conformation of the protein-active pharmaceutical ingredient (API) complex. The binding constant calculated through UV analysis was  $1.1 \times 10^4 \text{ M}^{-1}$ . Fluorescence spectroscopic analysis derived a value of  $1.7 \times 10^5 \text{ M}^{-1}$ .

1  
2  
3  
4 33 <sup>1</sup>. At the same time, DynamicBind predicted the cLDDT score for the top predicted model to  
5 34 be 0.634, and a binding affinity value of greater than 5, indicating a relatively moderate binding  
6 35 between Pioglitazone and HSA. The results from molecular dynamics simulations further  
7 36 complemented our earlier observations, indicating non-covalent binding interactions and a  
8 37 stable protein-API complex, which is desirable for developing a formulation using HSA as a  
9 38 carrier polymer. This orthogonal approach also provided critical information on the fate of the  
10 39 API and possible considerations that needed to be made during the design of the formulation  
11 40 process, highlighting the need for similar approaches that could provide multifaceted  
12 41 advantages and help in optimising R&D costs and timelines.

13  
14  
15  
16  
17  
18  
19  
20 42 **Keywords:** Orthogonal approach, Spectroscopy, Binding affinity, Deep-learning AI model,  
21 43 Molecular Dynamics, Molecular Docking.



## 451. Introduction

46 In the Generic Drug User Fee Act (GDUFA) Fiscal Year 2025 report, the U.S. Food and Drug  
47 Administration (US FDA) highlighted the development of orthogonal methods as a key  
48 investment area. In previous guidance documents for the characterization of drugs and  
49 biologics, the agency has emphasized the need for orthogonal methods as part of additional  
50 techniques.<sup>1</sup> This focus is also reflected in ICH guidelines, which have shaped the global  
51 understanding of orthogonal and complementary techniques for drug and biologic  
52 characterization.<sup>2</sup>

53 Orthogonal techniques have been critical to elucidate the structural and functional  
54 characteristics of drugs and formulations, especially in cases where a single analytical  
55 technique is unable to provide a complete dataset. With the advancements in drug formulation  
56 and the development of nanomaterials, the emphasis on advanced techniques to characterize  
57 individual critical quality attributes (CQAs) has become an area of research interest and is now  
58 a crucial part of regulatory submissions. Structure elucidation, drug-polymer binding, and the  
59 nature of bonds have also been evaluated in numerous articles and reports.<sup>3-8</sup>

60 In the study, we aimed to assess the binding of Pioglitazone drug to human serum albumin  
61 (HSA) using two different analytical techniques and two simulation tools. The objective was  
62 to verify whether we can use HSA to formulate a polymeric nanoparticle of Pioglitazone. HSA  
63 nanoparticles have been widely used to increase the solubility of poorly soluble drugs and  
64 enhance their pharmacokinetic behaviour *in vivo*.<sup>9,10,11</sup> It has also been used as a targeted drug  
65 delivery system owing to its propensity to be internalized in tumour sites.

66 The analytical techniques used for the study were UV spectroscopy and Fluorescence  
67 spectroscopy. Both techniques are spectroscopic in nature but use two different measuring  
68 principles. Through our analysis, we tried to determine whether the two analytical techniques  
69 can provide comprehensive information on the binding affinity of the drug to HSA, thereby  
70 aiding our understanding of the possible *in vivo* behaviour of the formulation.<sup>12,13</sup>

71 Alongside the two spectroscopic techniques, we performed molecular docking with a deep  
72 learning artificial intelligence (AI) docking tool, DynamicBind,<sup>14</sup> and Molecular dynamics  
73 simulation using Desmond in Schrodinger Release 2021-1, to understand the binding efficiency  
74 between HSA and Pioglitazone. Previously reported studies considered protein to be of a static  
75 nature, which is not the case.<sup>12,13,15,16</sup> In our study, both the simulation tools considered the  
76 protein to be in a dynamic state, and the simulation runs took into account the natural motion



1  
2  
3 77 of the protein and further equilibrated the system to derive the stable conformation, potentially  
4 aligning with actual observations.<sup>17,18</sup> May Article Online  
DOI: 10.1039/D3AY01534K

## 79 **2. Materials & Methods**

### 80 **2.1. Materials**

81 Vials containing Human serum albumin (20% solution, Grifols) and Pioglitazone  
82 hydrochloride (gift sample from Dr. Reddy's Laboratories Ltd.) were used to prepare the  
83 diluted albumin-bound Pioglitazone nanoparticle. Methanol (Rankem) and Acetone (Merck)  
84 were used as process solvents to dissolve the poorly soluble Pioglitazone HCl. A Jasco V-750  
85 double-beam spectrophotometer was used for UV analysis, and a Horiba Fluorolog 3-21 was  
86 employed for fluorescence spectroscopy.

### 87 **2.2. Methods**

#### 88 *2.2.1. Sample preparation*

89 A 12  $\mu\text{M}$  stock solution of HSA was prepared for both spectroscopic techniques. A  
90 Pioglitazone HCl stock solution was also prepared by dissolving the drug in a 4:1 mixture of  
91 Methanol and Acetone to attain a 5 mg/mL concentration. Next, 2 mL centrifuge tubes were  
92 filled with the HSA and Pioglitazone stock solutions in different combinations. The  
93 Pioglitazone concentrations in the centrifuge tubes ranged between 4.45 and 26.7  $\mu\text{g/mL}$ . The  
94 mixtures were vortexed for 1 min and analysed immediately.

#### 95 *2.2.2. UV Spectrophotometry analysis*

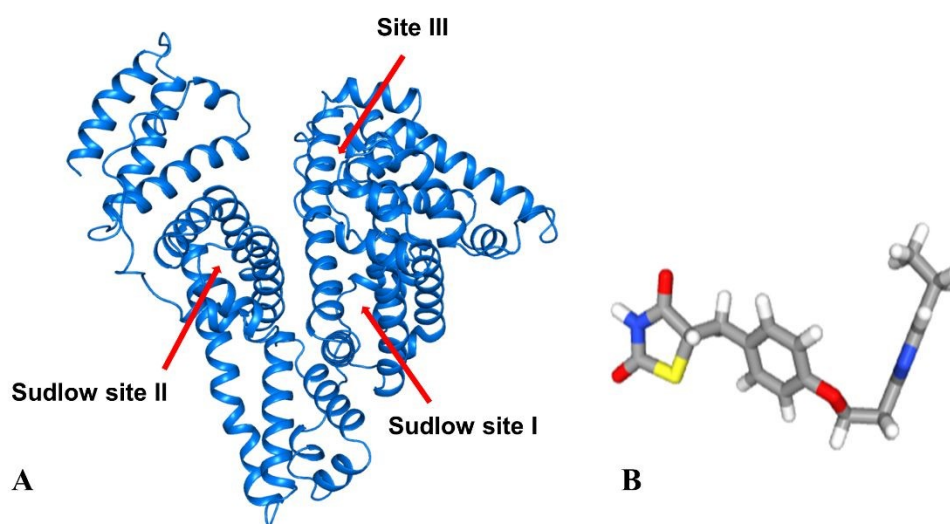
96 Each sample was analysed using a Double-beam UV Spectrophotometer (Jasco V-750  
97 Spectrophotometer). The blank contained the combination solution of Methanol and Acetone.  
98 In the sample cuvette, the different API-HSA complexes were transferred and then scanned for  
99 absorbance spectra between 200 and 400 nm with data points collected every 1 nm using  
100 application software Spectra Manager<sup>TM</sup>. The absorbance and  $\lambda_{\text{max}}$  were noted for each complex  
101 and HSA alone. The data were next plotted as a double reciprocal graph with absorbance values  
102 at 275 nm, the  $\lambda_{\text{max}}$  for HSA alone being used for calculation. Based on the equation for the  
103 graph plotted, the binding constant was deduced by dividing the intercept value by the slope  
104 value.<sup>15,16</sup>

#### 105 *2.2.3. Fluorospectrometric analysis*

1  
2  
3 106 Steady-state fluorescence spectroscopy was performed using a Horiba Fluorolog  
4 spectrophotometer. An excitation wavelength of 275 nm was applied for both HSA and API-  
5 107 spectrophotometer. An excitation wavelength of 275 nm was applied for both HSA and API-  
6 108 HSA complexes. Using the Horiba Fluorolog spectrophotometer, the emission spectra were  
7 109 analysed for HSA alone and all the combinations of API-HSA complexes. Like UV  
8 110 spectroscopy data, the Emission spectra were plotted as a double reciprocal graph with  
9 111 emission values at 361 nm, the emission max wavelength for HSA alone. Based on the equation  
10 112 for the graph plotted, the binding constant was deduced by dividing the intercept value by the  
11 113 slope value.

#### 114 2.2.4. Molecular Docking study: DynamicBind simulation

115 Molecular docking is an important approach to understanding protein-ligand interactions.<sup>19,20</sup>  
116 DynamicBind performs dynamic docking by allowing significant protein conformational  
117 changes to predict protein-ligand complexes. In this study, the Neurosnap platform was used  
118 to perform the AI-based simulation to bind Pioglitazone to HSA.<sup>21</sup> The protein structure of  
119 HSA (**Figure 1A**) was retrieved from the Protein Data Bank (PDB), and the ligand structure  
120 (**Figure 1B**) was obtained from PubChem. (Upon submission of both input parameters in  
121 DynamicBind (accessed in the Neurosnap platform on February 18, 2025), docking simulation  
122 were performed yielding the top 10 predicted protein-ligand models. The predicted structures  
123 were also complemented by their contact-LDDT (cLDDT) scores and binding affinity value,  
124 which were generated as part of the algorithm.<sup>14</sup>



125  
126 **Figure 1.** Structures of (A) human serum albumin (PDB ID 1AO6) and (B) Pioglitazone  
127 (PubChem CID 4829).

#### 128 2.2.5. Molecular Dynamics (MD) Simulation study

1  
2  
3 129 Molecular Dynamics simulation study was performed using the Desmond (D. E. Shaw  
4 Research, New York, Academic License, link: <https://www.deshawresearch.com/>) in  
5 Schrodinger Release 2021-1 to understand the dynamic interactive behaviour of the protein-  
6 ligand system.<sup>22</sup> As per standard protocol, the protein-ligand system built up by Desmond  
7 software was solvated with the TIP3P water model within a predefined orthorhombic box of  
8 10 Å size. This was followed by neutralization of the charges with an adequate quantity of  
9 counter ions. Further energy de-escalation was performed by removing steric clashes and other  
10 unfavourable interactions. As a final step, the energy-minimized system was loaded for a  
11 simulation run for 200 ns at 300 K, with a recording interval of 200 ps as per the NPT ensemble  
12 method. The output of the simulation runs was next interpreted in terms of radius of gyration  
13 (RG), root-mean square deviation (RMSD), and root-mean square fluctuation (RMSF).<sup>23</sup>  
14 Additionally, the free binding energy for the apo protein and protein-ligand complex was next  
15 calculated using the molecular mechanics with the generalized born and surface area solvation  
16 (MMGBSA) method.<sup>24,25</sup>

### 143 3. Results & Discussion

144 For macromolecules like HSA, fluorescence behaviour can help early researchers understand  
145 the molecular interaction between molecules of interest and HSA. Parameters that can be  
146 ascertained through fluorescence studies include binding affinity, binding mechanism, and the  
147 ligand binding site on the protein. Spectroscopic studies have played a significant role in  
148 annotating this behaviour. It has also been used to interpret the conformational changes the  
149 protein undergoes for binding to the protein.<sup>12,15,16,23-29</sup>

150 HSA is a 585 amino acid monomeric protein consisting of 17 disulfide bridges, with its  
151 secondary structure chiefly composed of  $\alpha$ -helices. HSA (**Figure 1A**) consists of 9 loops,  
152 spanning three homologous domains named Domain I (residues 1-195), II (residues 196-383),  
153 and III (residues 384-585), with each domain consisting of two long and one short loop. Each  
154 domain is further divided into two subdomains, with the first two loops denoted as subdomain  
155 A, with the remaining being denoted as subdomain B. HSA contains 35 cysteine residues, of  
156 which all, except the C34 residue in Domain I, are involved in a disulfide bond, further  
157 stabilizing the protein structure. Although these homologous domains appear to have similar  
158 structures, each domain exhibits distinct binding characteristics.<sup>23,30-33</sup>

159 It contains two major drug-binding sites: Sudlow site I (subdomain IIA), which preferentially  
160 binds bulky heterocyclic compounds, and Sudlow site II (subdomain IIIA), which favors



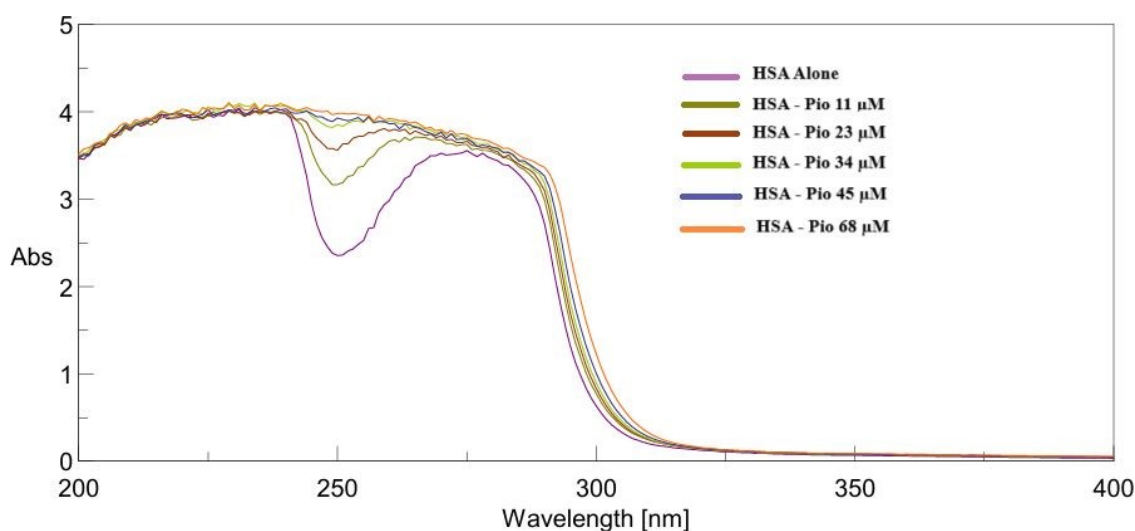
1  
2  
3 161 aromatic compounds. In addition, a third major non-Sudlow binding site has been identified in  
4 subdomain IB, capable of accommodating a wide range of endogenous and exogenous ligands.  
5 162 Albumin also possesses up to seven binding sites for long-chain fatty acids, each with distinct  
6 163 binding affinities.<sup>33</sup>  
7 164

8  
9  
10 165 In the present study, subdomain IIA (Sudlow site I) is of particular interest because pioglitazone  
11 166 contains a 2,4-thiazolidinedione ring and a pyridine moiety, structural features that favour  
12 167 binding at this site. HSA exhibits intrinsic fluorescence arising from three amino acid residues  
13 168 (tryptophan, tyrosine, and phenylalanine). Among these, tryptophan is the dominant  
14 169 fluorophore, and Sudlow site I is enriched with the key residue W214. The fluorescence  
15 170 contribution of phenylalanine is minimal, while tyrosine fluorescence is often diminished due  
16 171 to ionization and interactions with neighbouring amino and carboxyl groups, including  
17 172 proximity to tryptophan. Consequently, fluorescence quenching experiments primarily probe  
18 173 interactions involving W214 in subdomain IIA, enabling precise characterization of ligand  
19 174 binding at Sudlow site I.<sup>12,34</sup> Additionally, binding of small molecule drugs may not fill the  
20 175 hydrophobic pocket of the Sudlow site I, thereby predisposing the site to be filled with water  
21 176 molecules, and further Hydrogen bond interaction with the polar residues at the site.<sup>33,35</sup>

### 22 177 3.1. UV Spectrophotometry analysis

23 178 UV spectroscopic analysis is a simple and effective process to qualitatively and quantitatively  
24 179 measure the binding nature between protein and ligand. UV analysis of HSA alone revealed a  
25 180  $\lambda_{\text{max}}$  at 275 nm. Further analysis of the HSA-drug complexes revealed a blueshift of the UV  
26 181 spectrum (**Figure 2**). This indicated an interaction between the amino acids in the hydrophobic  
27 182 pocket and those of Pioglitazone. The hypsochromic spectrum shift is predominantly  
28 183 associated with the structural changes that the protein undergoes to accommodate the ligand to  
29 184 its preferred binding site. This phenomenon has been widely reported in multiple literatures  
30 185 and can be considered a cornerstone for structural analysis of protein-ligand complexes.<sup>15,16,30</sup>  
31 186 Besides the shift in the UV spectrum, a proportional increase in absorption intensity was also  
32 187 observed. An increase in intensity with an increase in drug concentration could also be  
33 188 attributed to the presence of Pioglitazone. Pioglitazone has a  $\lambda_{\text{max}}$  of 265 nm.<sup>35,36</sup> In general,  
34 189 the presence of ligand accentuates the blueshift, but in this specific case, it also contributes to  
35 190 the absorption intensity for the drug-protein complexes. The increase in intensity due to higher  
36 191 concentrations of the drug can indicate that the drug itself did not undergo any change and was  
37 192 able to hold on to its functional groups. It may also point to the fact that the binding of

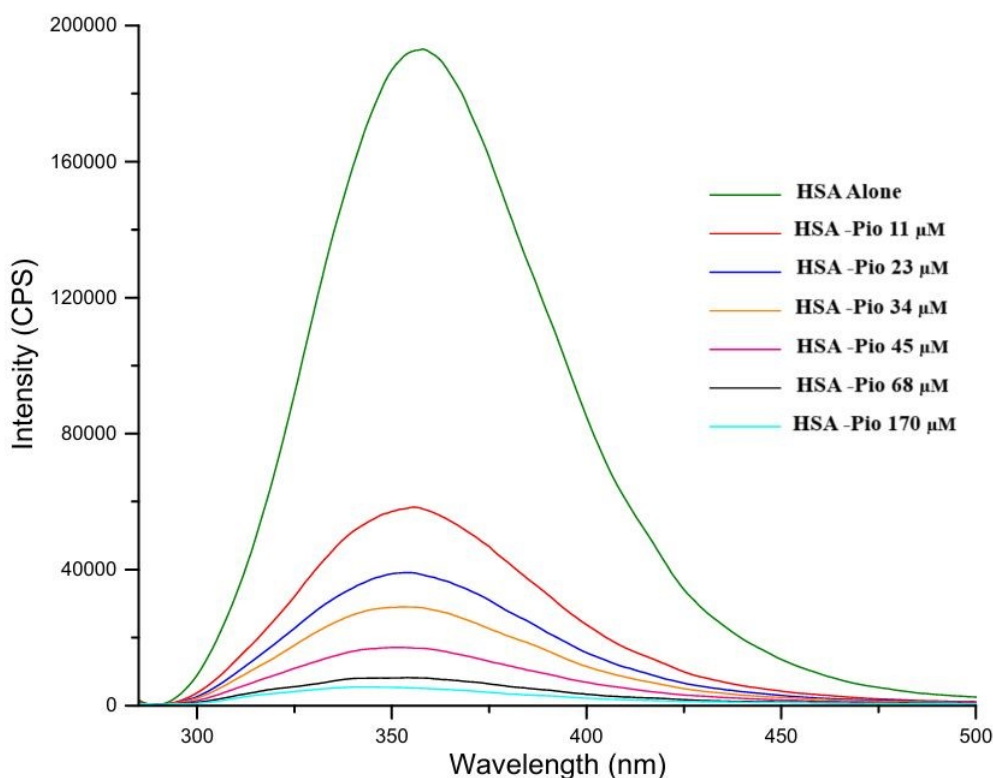
1  
2  
3 193 pioglitazone to the amino acid residues is non-covalent and the occurrence of a  $\pi$ - $\pi$  transition  
4  
5 194 with the Tryptophan residues at the binding site.<sup>19</sup>  
6  
7  
8  
9  
10  
11  
12  
13  
14  
15  
16  
17  
18  
19  
20  
21  
22  
23  
24  
25  
26  
27  
28  
29  
30  
31  
32  
33  
34  
35  
36  
37  
38  
39  
40  
41  
42  
43  
44  
45  
46  
47  
48  
49  
50  
51  
52  
53  
54  
55  
56  
57  
58  
59  
60



195  
196 **Figure 2.** The overlay of the UV spectra shows the hypsochromic shift of the absorbance for  
197 the different samples, with the  $\lambda_{\max}$  shifting to shorter wavelengths with increasing  
198 concentration and higher absorbance.  
199

### 200 3.2. Fluorospectrometric analysis

201 The fluorometric analysis involves quantifying photoluminescence triggered by the absorption  
202 of UV wavelengths. As previously established, HSA exhibits known photoluminescence  
203 properties, primarily due to the presence of Tryptophan residues. A spectroscopic analysis of  
204 HSA alone revealed that an excitation wavelength of 275 nm at room temperature generated  
205 an emission spectrum with a  $\lambda_{\max}$  at 361 nm. Like UV spectroscopy, fluorometric analysis  
206 generated emission spectra for individual drug-HSA complexes and a similar hypsochromic  
207 shift (**Figure 3**). On the other hand, the emission intensity showed a behaviour opposite to that  
208 of UV spectroscopy. Pioglitazone does not possess any fluorophore and hence did not  
209 contribute to the fluorescence intensity. The decline in intensity can be attributed to the  
210 utilization of tryptophan residues and adjacent amino acid residues for binding to pioglitazone.  
211 The inverse relationship proved the preferred binding site to be Sudlow site I for  
212 Pioglitazone.<sup>37-40</sup>



213

214 **Figure 3.** The overlay of the Emission spectra shows the hypsochromic shift of the  
 215 fluorescence for the different samples, with the emission max shifting to shorter wavelengths  
 216 with increasing concentration and lower fluorescence.

217

### 218 3.3. Double-reciprocal graphs to determine binding constant

219 A double reciprocal graph with respect to Pioglitazone molar concentration was plotted to  
 220 determine the binding constant. For UV spectroscopy (**Figure 4**), the mode values of  $1/(A_0-A)$   
 221 were considered for plotting the graph and plotted with regard to the inverse of the molar  
 222 concentration of Pioglitazone in the samples. For Fluorescence spectroscopy (**Figure 5**), the  
 223  $1/(E_0-E)$  values were plotted vs the reciprocal of Pioglitazone molar concentration of samples.  
 224 In respective cases,  $A_0$  and  $E_0$  indicated the absorbance for HSA alone at 275 nm and the  
 225 emission of HSA alone at emission wavelength 361 nm. The spectroscopic titration by  
 226 individual methods was performed for individual concentrations at the aforementioned  
 227 wavelengths for respective methods. For Fluorescence spectroscopic titration, an emission/  
 228 fluorescence correction ( $E_{cor}$ ) was done, considering the inner filter effect study, as per  
 229 Equation 1, where absorbance values of Pioglitazone at excitation ( $A_{ex}$ ) and emission ( $A_{em}$ )  
 230 wavelength were considered for the correction  $E_{obs}^{41}$



$$E_{cor} = E_{obs} * 10^{\frac{A_{ex}}{2} + \frac{A_{em}}{2}} \dots \text{Equation 1}$$

View Article Online  
DOI: 10.1039/D5AY01534K

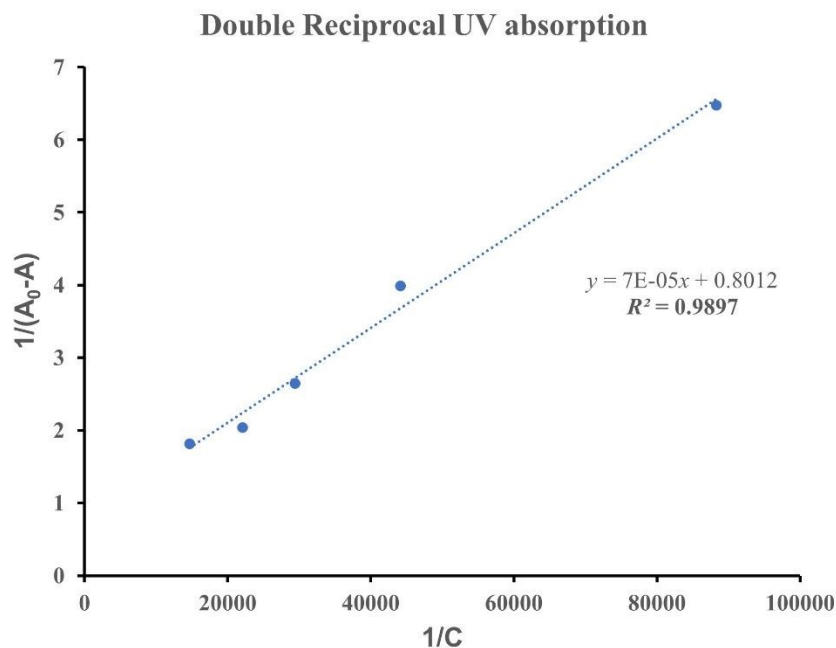


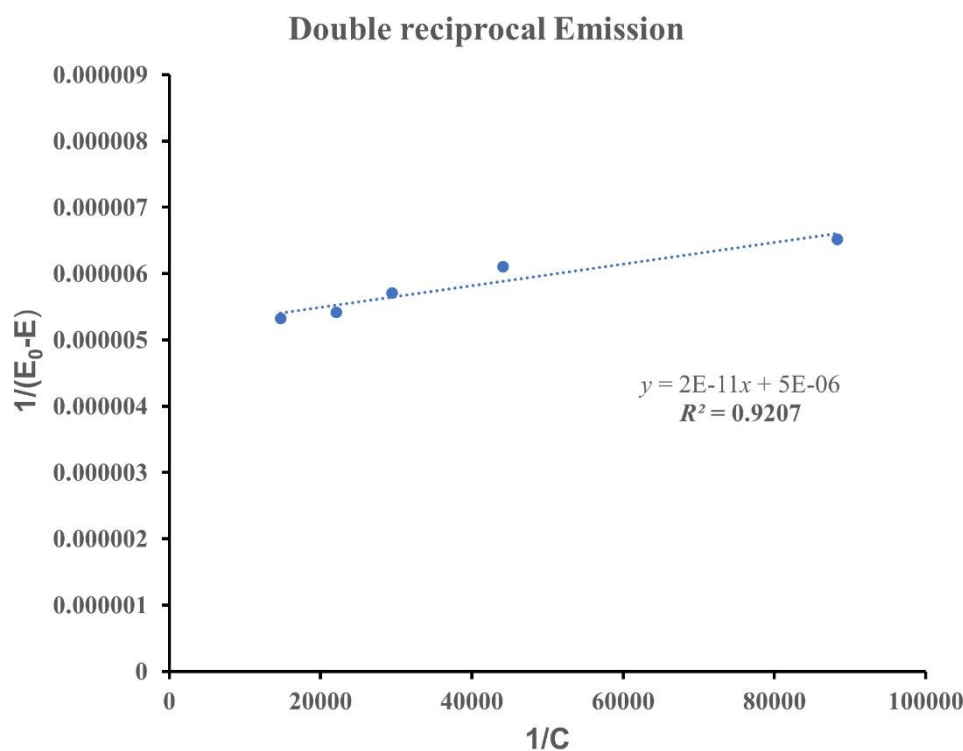
**Figure 4.** The double reciprocal graph of UV absorbance with different HSA-Pioglitazone complexes.

The plotted graph showcased a linear relationship with a correlation coefficient higher than 0.9 for both spectroscopic procedures. The binding constant derived from the graph was next calculated by dividing the intercept value by the slope of the graph. The binding constant calculated through UV analysis had a value of  $1.1 \times 10^4 \text{ M}^{-1}$ , while Fluorescence spectroscopic analysis derived a value of  $1.7 \times 10^5 \text{ M}^{-1}$ . Both these values are indicative of medium affinity (expected values to be between  $10^3$  and  $10^6 \text{ M}^{-1}$ ).<sup>12,15,16,37,39</sup>

The binding affinity of a drug to the protein site can influence its therapeutic effectiveness in vivo. The ability of a drug to diffuse from systemic circulation and reach its intended target depends much on its binding affinity to plasma proteins like HSA. Our study aimed to evaluate the binding affinity and nature of interactions of Pioglitazone to HSA. A drug weakly bonded to HSA will have poor bioavailability as it will be poorly distributed, rapidly metabolised, and eliminated, thereby having a shorter half-life. Strongly bonded drugs, in contrast, will not be efficiently released to be available, resulting in sub-therapeutic effectiveness. Moderately bonded drugs ensure that the drug will efficiently diffuse through the biological barrier and have the required half-life to be transported through the systemic circulation to its intended activity site. At the same time, the affinity does not impede its release, thereby ensuring the availability of the drug in sufficient concentration to exert its therapeutic impact. The binding



252 affinity values generated through the orthogonal studies complement the understanding with  
 253 regard to the values derived from spectroscopic measurements.<sup>15,16,30,38</sup>



254  
 255 **Figure 5.** The double reciprocal graph of Fluorescence emission with different HSA-  
 256 Pioglitazone complexes.

### 257 258 3.4. *DynamicBind simulation*

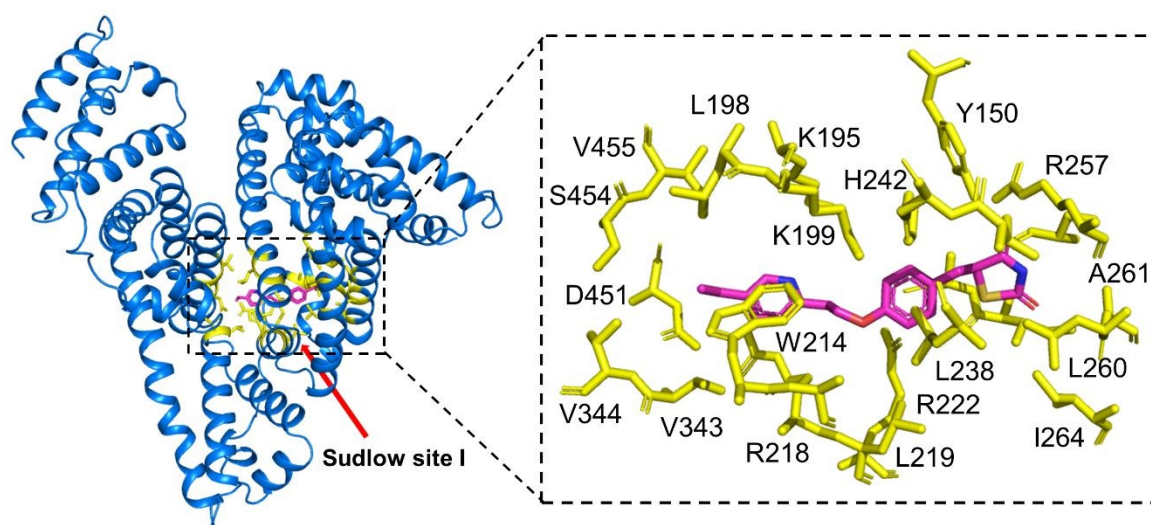
259 DynamicBind is a geometric deep generative model that considers proteins not to be in a state  
 260 of rigid configuration while docking.<sup>14</sup> This ability of proteins to transition between multiple  
 261 conformations is central to their functional character *in vivo*. Ligands, especially drug moieties,  
 262 can only bind to specific conformations of the targeted protein molecule, thereby regulating  
 263 the overall impact of the drug in the biological system. It outperforms other models in  
 264 predicting possible ligand poses for known protein datasets (PDB and MDT). It does so by  
 265 being able to predict protein configuration with lower Root Mean Square Deviation (RMSD)  
 266 scores for regions around the binding sites, providing a protein conformation resembling its  
 267 native state. The cLDDT scoring developed as a measuring parameter for DynamicBind  
 268 generated models is well aligned with the auROC score, showing its effectiveness in selecting  
 269 the most appropriate model from amongst its multiple predicted protein-ligand complexes.  
 270 DynamicBind also calculates Binding affinity as a negative logarithm value of dissociation and

1  
 2  
 3  
 4  
 5  
 6  
 7  
 8  
 9  
 10  
 11  
 12  
 13  
 14  
 15  
 16  
 17  
 18  
 19  
 20  
 21  
 22  
 23  
 24  
 25  
 26  
 27  
 28  
 29  
 30  
 31  
 32  
 33  
 34  
 35  
 36  
 37  
 38  
 39  
 40  
 41  
 42  
 43  
 44  
 45  
 46  
 47  
 48  
 49  
 50  
 51  
 52  
 53  
 54  
 55  
 56  
 57  
 58  
 59  
 60

271 complements the cLDDT score to assess the quality of ligand interaction with the protein  
 272 binding site.<sup>14,42</sup>

273 The DynamicBind predicted the cLDDT score for the top predicted model to be 0.634, with  
 274 the range varying between the top model between 0.634-0.472, with the absolute value of 1  
 275 indicative of near native contact.<sup>21</sup> The binding affinity value greater than 5 indicates a  
 276 relatively moderate binding between Pioglitazone and HSA.<sup>43</sup> The results are consistent with  
 277 the practical observations from the spectroscopy analysis, where we predicted the affinity to  
 278 be of medium intensity. Therefore, DynamicBind can serve as a usable tool for initial screening  
 279 and understanding. The fact that it demands far less computational power compared to  
 280 conventional docking tools, makes it lucrative for researchers working on early-stage projects.

281 Aside from the binding interaction deduced through spectroscopic analysis, the simulated  
 282 docking study also identified other interactions and their nature. A  $\pi$ - $\pi$  stacked interaction is  
 283 evident between the pyridine ring and the tryptophan residue (W214), with the electron-rich  
 284 indole ring of tryptophan contributing to such non-covalent interactions, inadvertently  
 285 stabilizing the protein-ligand system (**Figure 6**).



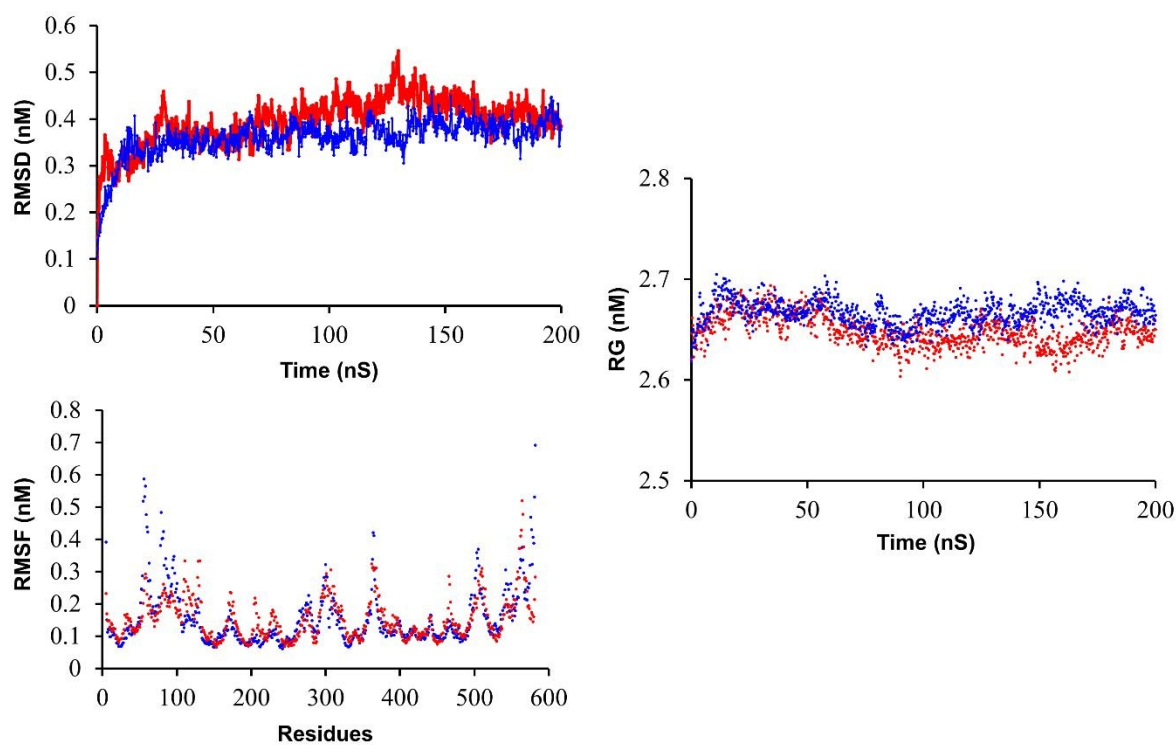
286  
 287 **Figure 6.** Possible binding mode of Pioglitazone (shown as a pink stick model) within the  
 288 binding site of human serum albumin (HSA, shown as a cartoon representation). Interacting  
 289 residues are highlighted in yellow.

291 A  $\pi$ -alkyl interaction between W214 and the alkyl chain adjacent to pyridine is also predicted,  
 292 owing again to the indole group of W214.<sup>44,45</sup> The other predicted interaction involving amino  
 293 acid residues other than W214 includes a  $\pi$ -cation interaction of the pyridine ring of

294 Pioglitazone with arginine residue (R218) owing to the positively charged guanidinium  
 295 group,<sup>46</sup> a  $\pi$ -alkyl interaction between the benzene ring of Pioglitazone and leucine residue  
 296 (L238), and a hydrogen bond between R257 residue and the thiazolidinedione ring  
 297 (**Supplementary Figure S1**). The possible nature of binding interactions is thereby non-  
 298 covalent, further supporting our earlier assumptions derived from the previously executed  
 299 studies.

### 300 3.5. Molecular dynamics (MD) Simulation study

301 The molecular dynamics simulation was run for a period of 200 ns, and the stability of the  
 302 protein-API system was assessed. The assessment was done on the RG, RMSD, and RMSF  
 303 values derived for the protein in both the apo and bound states. The RMSD values, as observed  
 304 from **Figure 7**, indicate that the protein-ligand system is as stable as the apo-protein structure,  
 305 while the RG values for both protein systems show similar compactness, corroborating the  
 306 previous observation obtained through DynamicBind simulation. The residual mobility of the  
 307 bounded and unbounded form of human serum albumin was further computed, and the  
 308 resulting RMSF values for the residue seem to be comparable with the apo protein, showing  
 309 more structural flexibility than the bounded form.<sup>47,48</sup>



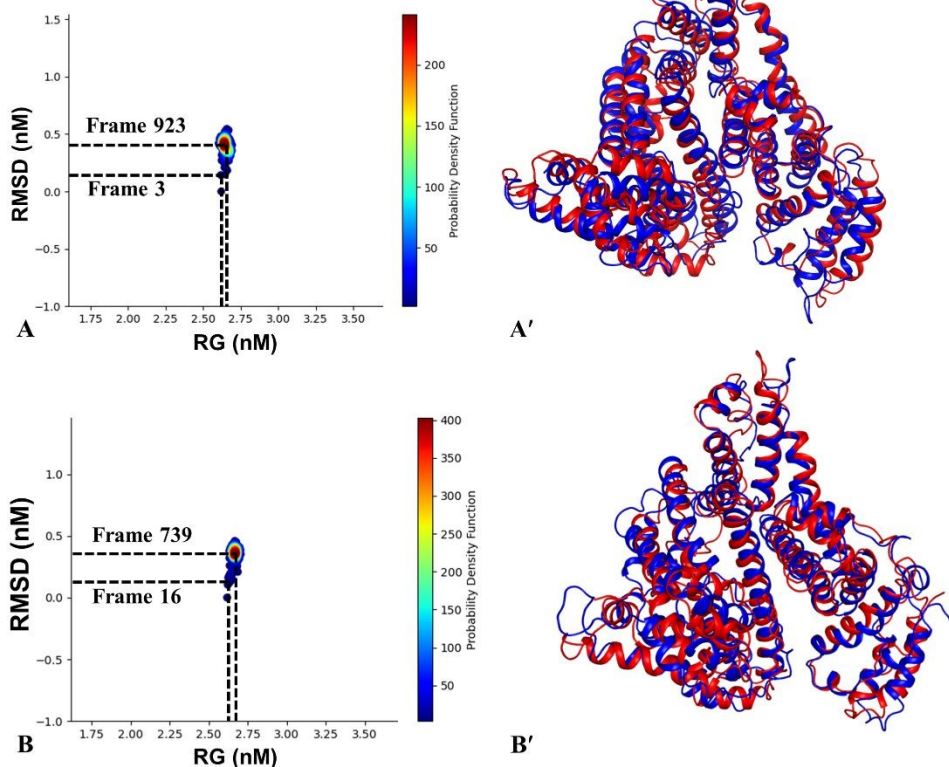
310  
 311 **Figure 7.** Comparison of RMSD, RMSF, and RG of apo-human serum albumin (blue) and its  
 312 complexes with Pioglitazone (red).

1  
2  
3 313 Hydrogen-bond analysis of the MD trajectory revealed stable and persistent interactions  
4 between Pioglitazone and key HSA residues. R257 exhibited the highest hydrogen-bond  
5 314 occupancy (~77%), followed by S287 (~34%) and R222 (~16%), indicating their critical roles  
6 315 in ligand stabilization. Additional hydrogen-bond interactions were observed with R218  
7 316 (~13%), L260 (~8%), and A261 (~1%). As shown in **Supplementary Figure S2**, the timeline  
8 317 analysis illustrates the dynamic evolution of Pioglitazone-HSA interactions, highlighting both  
9 318 the overall interaction frequency and residue-wise contact persistence throughout the  
10 319 simulation. Collectively, the high occupancy and temporal stability of these hydrogen bonds  
11 320 support the favourable binding orientation of Pioglitazone and confirm the dynamic stability  
12 321 of the Pioglitazone-HSA complex during the MD simulation.  
13 322

### 14 323 *3.6. Probability density function (PDF) analysis*

15 324 The Probability Density Function plots analysed the different conformations of the apo and  
16 325 ligand-bound protein. They mapped them based on the highest (in blue) and lowest (in red)  
17 326 occurring conformations (**Figure 8**). The differences in RMSD value between the highest and  
18 327 lowest conformers for both the apo protein seemed to be higher than that of the ligand-bound  
19 328 protein, indicating a higher flexibility for the unbound protein than that of the bound protein.  
20 329 In case of RG values, the differences between the highest and lowest conformers of the apo-  
21 330 protein seem to be narrower than those for the API bound protein, indicating structural changes  
22 331 and slight relaxation of the protein secondary structure.<sup>47,49</sup>





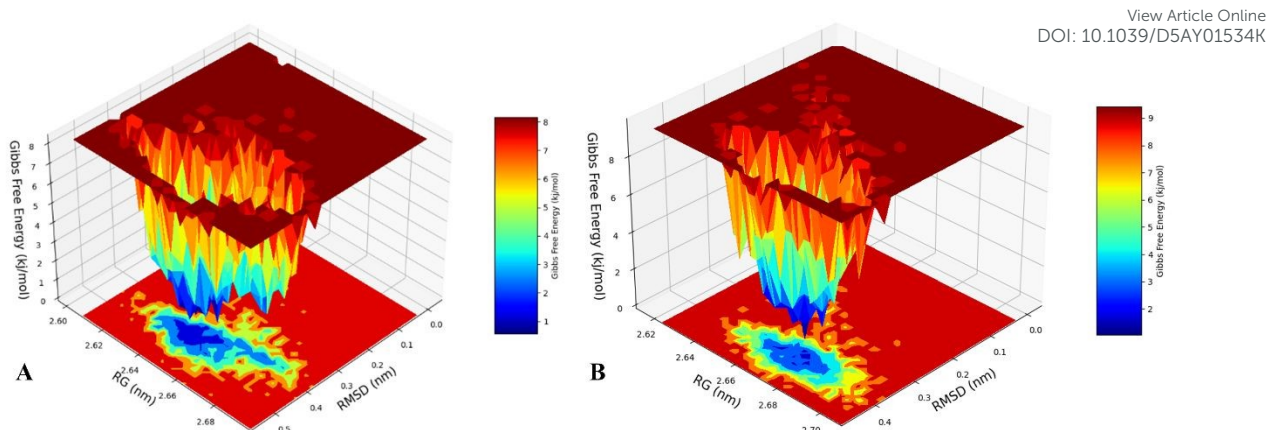
332

333 **Figure 8.** Probability density function (PDF) plot along with corresponding largest (blue),  
 334 sparsely populated (red) conformation in case of apo-HSA (A, A'), Pioglitazone-bound HSA  
 335 (B, B').

### 336 3.7. 3D Free Energy Landscape (FEL) analysis

337 The 3D FEL plots (**Figure 9**) were prepared to map the free energy variation in accordance  
 338 with the RMSD and RG values for different conformations of the unbound (apo) and bound  
 339 protein conformations. The 3D plot for the apo protein showcased a wider cluster of low-energy  
 340 peaks, which may be a result of multiple conformations being in a metastable state, owing to  
 341 the absence of a ligand to restrict the apo protein to a stable conformer (**Figure 9A**). On the  
 342 other hand, a narrow cluster of low-energy peaks was derived for the API-bound protein  
 343 complex, indicating a more stable conformation (**Figure 9B**). The observations were  
 344 comparable to those observed through PDF analysis and further demonstrate the correlation  
 345 between RMSD and RG values to free energy variation, to deduce conformer stability.<sup>47,49</sup>

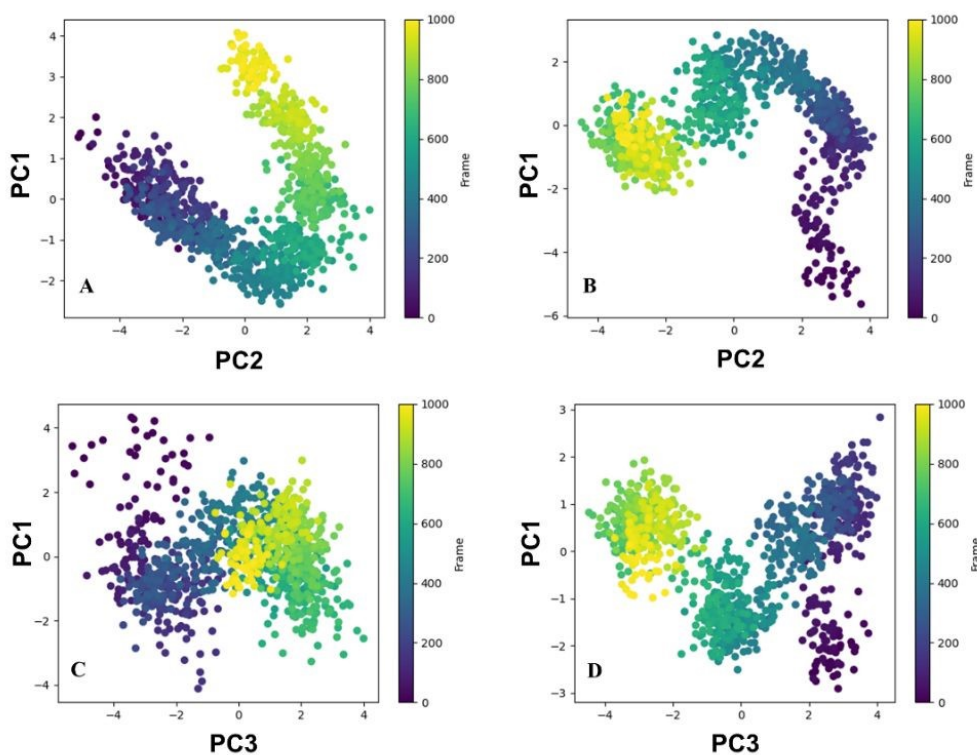




346  
347 **Figure 9.** Free energy landscape (FEL) plot of (A) apo-HSA, and (B) Pioglitazone-bound HSA.

### 348 3.8. Principal Component Analysis (PCA)

349 Furthermore, principal component analysis of the MD trajectory data was performed to account  
350 for any alteration in the major global atomic motion of amino acid residues in unbound (apo)  
351 and bound HSA. The coherent internal 3D motions were captured using a covariance matrix,  
352 with the resulting eigenvectors representing dominant modes of motion in the trajectory.  
353 Notable differences in trajectory clustering were observed for both the unbound (apo) and  
354 bound protein (**Figure 10**).



355  
356 **Figure 10.** PCA plot for [A/C] for HSA and [B/D] for Pioglitazone-bound HSA.

357 In the case of apo-HSA, all intermediate frames (excluding initial frames) clustered along PC1  
358 vs. PC2, indicating global conformational shifts. Interestingly, the terminal frames (800-1000)  
359 of the Pioglitazone-bound HSA complex scattered together, suggesting a trend toward  
360 convergence, unlike the more dispersed apo structure. Meanwhile, in the PC1 vs. PC3  
361 projection, the terminal apo-HSA frames aligned along PC3, indicating subtle side-chain  
362 rearrangements (**Figure 10**). These shifts likely reflect the presence of multiple low-energy  
363 conformers, consistent with findings from previous FEL analyses (**Figure 9**).

#### 364 4. Conclusion

365 In this study, we tried to assess the implementation of a few simple techniques to determine  
366 the tested parameter. The spectroscopic techniques discussed are commonly available  
367 instruments. Compared with advanced tools such as nuclear magnetic resonance, our  
368 approaches require simpler sample preparation, instrument handling, and data interpretation,  
369 making them more feasible for early-stage researchers. Notably, this study employed a deep  
370 learning-based artificial intelligence framework to perform non-conventional, dynamic  
371 molecular docking. In contrast to similar-type of previously reported studies<sup>40,50</sup> that typically  
372 treat HSA as rigid entities, the present work considers the HSA in a dynamic state during  
373 docking. Furthermore, the use of DynamicBind via the user-friendly Neurosnap platform  
374 eliminates the need for high-performance computing resources, thereby broadening  
375 accessibility to the wider research community. Complementary 200 ns molecular dynamics  
376 simulations provided additional insights into binding efficiency, protein-ligand complex  
377 stability, and conformational behavior, collectively strengthening the reliability and  
378 mechanistic interpretation of the results.

379 The understanding derived is pivotal for designing formulation strategy and predicting  
380 probable behaviour of the formulated product involving HSA as a carrier for Pioglitazone *in*  
381 *vivo*. The moderate binding affinity values of Pioglitazone to HSA, derived through  
382 spectroscopic techniques, further corroborated to an extent by the simulation tools, provided  
383 affirmative proof of the suitability for developing an HSA-bound formulation system. The  
384 spectroscopic analysis and docking study indicated that the binding between the drug and  
385 protein is non-covalent and exhibits the requisite affinity, which is expected to improve the  
386 drug's bioavailability. The simulated docking studies further shed light on the possible  
387 formulation pathway. The cLDDT score suggests that for the interaction to occur, a slight  
388 modification is required of the native protein conformation. These findings indicate that

1  
2  
3 389 incorporating an energy-input step into the process design may facilitate binding. Therefore,  
4 through this pre-formulation study, which aimed to determine the binding affinity via an  
5 390 orthogonal approach, we derived information that could help us design the process and predict  
6 391 *in vivo* behavior. It can also prove beneficial as it will help reduce R&D cost and timeline,  
7 392 showing the utility of orthogonal techniques beyond regulatory stipulations.  
8 393

#### 394 **Funding**

395 This research did not receive any specific grant from funding agencies in the public,  
396 commercial, or not-for-profit sectors.

#### 397 **CRedit authorship contribution statement**

398 **Saswata Banerjee:** Conceptualization, Methodology, Investigation, Data Curation, Formal  
399 Analysis, Writing- original draft, Visualization. **Sk. Abdul Amin:** Investigation, Data  
400 Curation, Formal Analysis, Writing- original draft, Visualization. **Shovanlal Gayen:** Data  
401 Curation, Formal Analysis, Writing- original draft, Supervision. **Gautam Singhvi:** Writing-  
402 review & editing, Supervision. **Rajeev Taliyan:** Writing- review & editing, Supervision.  
403 **Sakshi Priya:** Data Curation, Writing- review & editing. **Yashika Tomar:** Data Curation,  
404 Writing- review & editing.

#### 405 **Conflict of Interest**

406 There are no conflicts of interest to declare.

#### 407 **Acknowledgments**

408 This research received no external funding. The authors would like to thank and acknowledge  
409 Central Instrument Facility, BITS Pilani, Pilani campus, for allowing the use of its facilities  
410 and for providing access to the UV Spectrophotometer and Spectrofluorometer for analysis  
411 purposes. We sincerely acknowledge the Department of Pharmacy, University of Salerno, Italy,  
412 and the Department of Pharmaceutical Technology, Jadavpur University, India, for providing  
413 the research facilities.

#### 414 **Data availability**

415 The authors confirm that the data supporting the findings of this study are available within the  
416 article [and/or] its supplementary materials.

#### 417 **References**

- 1  
2  
3 418 1. U.S. Food and Drug Administration. FY 2025 GDUFA Science and Research Priority Initiatives. <https://www.fda.gov/drugs/generic-drugs/fy-2025-gdufa-science-and-research-priorities>. (Accessed on February 2026)
- 4 419  
5 420  
6 421 2. International Council for Harmonisation of Technical Requirements for  
7 422 Pharmaceuticals for Human Use (ICH). Validation of Analytical Procedures Q2(R2).  
8 423 [https://database.ich.org/sites/default/files/ICH\\_Q2-  
9 424 R2\\_Document\\_Step2\\_Guideline\\_2022\\_0324.pdf](https://database.ich.org/sites/default/files/ICH_Q2-R2_Document_Step2_Guideline_2022_0324.pdf) (Accessed on February 2026)
- 10 425 3. C.G. Simon, C.G., Borgos, S.E., Calzolari, L., Nelson, B.C., Parot, J., Petersen, E.J.,  
11 426 Roesslein, M., X., Caputo, F. Orthogonal and complementary measurements of  
12 427 properties of drug products containing nanomaterials, *Journal of Controlled Release*,  
13 428 2023, 354, 120-127.
- 14 429 4. E. Van Gyseghem, S. Van Hemelryck, M. Daszykowski, F. Questier, D.L. Massart, Y.  
15 430 Vander Heyden. Determining orthogonal chromatographic systems prior to the  
16 431 development of methods to characterise impurities in drug substances. *Journal of*  
17 432 *Chromatography A*. 2003 Feb 21;988(1):77-93.
- 18 433 5. K.M. Tyner, N. Zheng, S. Choi, *et al.* How Has CDER Prepared for the Nano  
19 434 Revolution? A Review of Risk Assessment, Regulatory Research, and Guidance  
20 435 Activities. *AAPS J*, 2017, 19, 1071–1083.
- 21 436 6. F. Caputo, J. Clogston, L. Calzolari, M. Rösslein, A. Prina-Mello. Measuring particle  
22 437 size distribution of nanoparticle enabled medicinal products, the joint view of EUNCL  
23 438 and NCI-NCL. A step by step approach combining orthogonal measurements with  
24 439 increasing complexity. *J. Control. Release*, 2019, 299, 31-43.
- 25 440 7. L. Newey-Keane. The Power Of Orthogonality In Assessing The Stability Of  
26 441 Biopharmaceuticals. [https://www.technologynetworks.com/analysis/news/the-power-  
27 442 of-orthogonality-in-assessing-the-stability-of-biopharmaceuticals-211659](https://www.technologynetworks.com/analysis/news/the-power-of-orthogonality-in-assessing-the-stability-of-biopharmaceuticals-211659) (Accessed  
28 443 on February 2026)
- 29 444 8. Yokogawa Fluid Imaging Technologies, Inc. Enhancing biotherapeutic research: The  
30 445 role of orthogonal and complementary analytical techniques. [https://www.news-  
31 446 medical.net/whitepaper/20240718/Enhancing-biotherapeutic-research-The-role-of-  
32 447 orthogonal-and-complementary-analytical-techniques.aspx](https://www.news-medical.net/whitepaper/20240718/Enhancing-biotherapeutic-research-The-role-of-orthogonal-and-complementary-analytical-techniques.aspx) (Accessed on February  
33 448 2026)
- 34 449 9. S. Tayyab, & S.R. Feroz. Serum albumin: clinical significance of drug binding and  
35 450 development as drug delivery vehicle. *Advances in protein chemistry and structural*  
36 451 *biology*, 2021, 123, 193-218.
- 37 452 10. A.B. Gurung, M.A. Ali, J. Lee, M.A. Farah, K.M. Al-Anazi, H. Sami. Molecular  
38 453 modelling studies unveil potential binding sites on human serum albumin for selected  
39 454 experimental and in silico COVID-19 drug candidate molecules. *Saudi Journal of*  
40 455 *Biological Sciences*, 2022, 29(1), 53-64.
- 41 456 11. H.Y. Tao, R.Q. Wang, W.J. Sheng, Y.S. Zhen. The development of human serum  
42 457 albumin-based drugs and relevant fusion proteins for cancer therapy. *International*  
43 458 *journal of biological macromolecules*, 2021, 187, 24-34.
- 44 459 12. H. Gao, L. Lei, J. Liu, Q. Kong, X. Chen, Z. Hu. The study on the interaction between  
45 460 human serum albumin and a new reagent with antitumour activity by  
46 461 spectrophotometric methods. *Journal of Photochemistry and Photobiology A:*  
47 462 *Chemistry*, 2004, 167(2–3), 213-221,  
48 463 <https://doi.org/10.1016/j.jphotochem.2004.05.017>.



- 1  
2  
3  
4  
5  
6  
7  
8  
9  
10  
11  
12  
13  
14  
15  
16  
17  
18  
19  
20  
21  
22  
23  
24  
25  
26  
27  
28  
29  
30  
31  
32  
33  
34  
35  
36  
37  
38  
39  
40  
41  
42  
43  
44  
45  
46  
47  
48  
49  
50  
51  
52  
53  
54  
55  
56  
57  
58  
59  
60
13. A.A. Salem, M. Lotfy, A. Amin, M.A. Ghattas. Characterization of human serum albumin's interactions with safranal and crocin using multi-spectroscopic and molecular docking techniques. *Biochem Biophys Rep.* 2019, 12, 20:100670. doi: 10.1016/j.bbrep.2019.100670. Erratum in: *Biochem Biophys Rep.* 2021 Jan 07;25:100901.
14. W. Lu, J. Zhang, W. Huang, Z. Zhang, X. Jia, Z. Wang, L. Shi, C. Li, P.G. Wolynes, S. Zheng. DynamicBind: predicting ligand-specific protein-ligand complex structure with a deep equivariant generative model. *Nat Commun.*, 2024, 15(1),1071. doi: 10.1038/s41467-024-45461-2.
15. A. Najmi, M. Albratty, H.A. Alhazmi, N. Thangavel, M.S. Alam, W. Ahsan, S.A. Javed, I.A. Arbab, K.A. El-Sharkawy. Spectroscopic and in silico approach to probe the binding interactions of irbesartan and human serum albumin. *Journal of King Saud University - Science*, 2022, 34(3). <https://doi.org/10.1016/j.jksus.2022.101875>
16. M.A. Bratty. Spectroscopic and molecular docking studies for characterizing binding mechanism and conformational changes of human serum albumin upon interaction with Telmisartan. *Saudi Pharmaceutical Journal*, 2020, 28(6), 729–736. <https://doi.org/10.1016/j.jsps.2020.04.015>
17. T. Sakano, M.I. Mahamood, T. Yamashita, H. Fujitani. Molecular dynamics analysis to evaluate docking pose prediction. *Biophysics and physcobiology*, 2016, 13, 181-194.
18. D. Gioia, M. Bertazzo, M. Recanatini, M. Masetti, A. Cavalli. Dynamic docking: a paradigm shift in computational drug discovery. *Molecules*, 2017, 22(11), 2029.
19. Y. Yue, Q. Tu, Y. Guo, Y. Wang, Y. Xu, Y. Zhang, J. Liu. Comparison of the interactions of fanetizole with pepsin and trypsin: spectroscopic and molecular docking approach. *J Mol Liq.*, 2022, 365:120095.
20. X. Wang, Y. Yue, Y. Zhang, Z. Wang, J. Liu, Q. Tang. Probing the interaction of pepsin with imidacloprid via DFT calculation, spectroscopic approaches and molecular docking. *J Mol Struct.*, 2019 1197,210-216.
21. Neurosnap Inc. - Computational Biology Platform for Research. Wilmington, D.E., 2022. <https://neurosnap.ai/>. (Accessed on February 2026)
22. K.J. Bowers, E. Chow, H. Xu, R.O. Dror, M.P. Eastwood, B.A. Gregersen, ... & D.E. Shaw. Scalable algorithms for molecular dynamics simulations on commodity clusters. In *Proceedings of the 2006 ACM/IEEE Conference on Supercomputing* (pp. 84-es).
23. P. Lee, & X. Wu. Modifications of human serum albumin and their binding effect. *Current pharmaceutical design*, 2015, 21(14), 1862-1865.
24. S. Khatun, R. Islam, S.A. Amin, A. Bhattacharya, D.K. Dhaked, T. Jha, T., & S. Gayen. Nitrogen-containing heterocycles as an important scaffold for selective and potent HDAC8 inhibition: a step towards effective, non-toxic and selective HDAC8 inhibitor discovery. *Journal of Biomolecular Structure and Dynamics*, 2024, 1-19.
25. L.P. Kagami, G.M. das Neves, L.F.S.M. Timmers, R.A. Caceres, V.L. Eifler-Lima. Geo-Measures: a PyMOL plugin for protein structure ensembles analysis. *Comput Biol Chem.*, 2020, 87:107322. doi:10.1016/j.compbiolchem.2020.107322.
26. A. Szkudlarek. Effect of palmitic acid on tertiary structure of glycosylated human serum albumin. *Processes*. 2023;11(9):2746.
27. S.A. Mardikasari, G. Katona, I. Csóka. Serum albumin in nasal drug delivery systems: exploring the role and application. *Pharmaceutics*. 2024;16(10):1322.

- 1  
2  
3 510 28. R. Vaidyanathan, S.M. Sreedevi, K. Ravichandran, S.M. Vinod, Y.H. Krishnan, J.K. Babu, ... & V. Mahalingam. Molecular docking approach on the binding stability of  
4 511 derivatives of phenolic acids (DPAs) with Human Serum Albumin (HSA): hydrogen-  
5 512 bonding versus hydrophobic interactions or combined influences?. *JCIS Open*,  
6 513 2023, 12, 100096.  
7 514  
8 515 29. M. Bteich. An overview of albumin and alpha-1-acid glycoprotein main characteristics:  
9 516 highlighting the roles of amino acids in binding kinetics and molecular  
10 517 interactions. *Heliyon*, 2019, 5(11).  
11 518  
12 519 30. X.Q. Zhou, B.L. Wang, S.B. Kou, Z.Y. Lin, Y.Y. Lou, K.L. Zhou, J.H. Shi. Multi-  
13 520 spectroscopic approaches combined with theoretical calculation to explore the  
14 521 intermolecular interaction of telmisartan with bovine serum albumin. *Chemical*  
15 522 *Physics*, 2019, 522, 285–293 <https://doi.org/10.1016/j.chemphys.2019.03.019>  
16 523  
17 524 31. S. Curry. Lessons from the crystallographic analysis of small molecule binding to  
18 525 human serum albumin. *Drug metabolism and pharmacokinetics*, 2009, 24(4), 342-357.  
19 526  
20 527 32. A. Sułkowska. Interaction of drugs with bovine and human serum albumin. *Journal of*  
21 528 *molecular structure*, 2002, 614(1-3), 227-232.  
22 529  
23 530 33. S. Sugio, A. Kashima, S. Mochizuki, M. Noda, K. Kobayashi. Crystal structure of  
24 531 human serum albumin at 2.5 Å resolution. *Protein engineering*, 2009, 12(6), 439-446.  
25 532  
26 533 34. National Center for Biotechnology Information (2025). PubChem Compound  
27 534 Summary for CID 4829,  
28 535 Pioglitazone. <https://pubchem.ncbi.nlm.nih.gov/compound/Pioglitazone>. (Retrieved  
29 536 on February 23, 2025)  
30 537  
31 538 35. S. Imre, D. Anghel, A. Pușcaș, A.G. Cârje, D.L. Muntean, A. Balint, ... & C. Toma.  
32 539 Contributions to quality control by HPLC of fixed combinations with pioglitazone and  
33 540 metformin. *Acta Medica Transilvanica*, 2023, 28(2).  
34 541  
35 542 36. United States Pharmacopoeia. 2016. Pioglitazone and Metformin Hydrochloride  
36 543 Tablets monograph. USP 40-NF 35. (Accessed on February 2026)  
37 544  
38 545 37. V. Rajendiran, R. Karthik, M. Palaniandavar, V.S. Periasamy, M.A. Akbarsha, B.S.  
39 546 Srinag. Mixed-ligand copper(II)- phenolate complexes: effect of coligand on enhanced  
40 547 DNA and protein binding, DNA cleavage, and anticancer activity. *Inorg. Chem.*, 2007  
41 548 46, 8208–8221. <https://doi.org/10.1021/ic700755p>.  
42 549  
43 550 38. C. Dufour, O. Dangles. Flavonoid-serum albumin complexation: determination of  
44 551 binding constants and binding sites by fluorescence spectroscopy. *BBA*, 2004, 1721,  
45 552 164–173. <https://doi.org/10.1016/j.bbagen.2004.10.013>.  
46 553  
47 554 39. J. Li, J. Li, Y. Jiao, C. Dong. Spectroscopic analysis and molecular modeling on the  
48 555 interaction of jatrorrhizine with human serum albumin (HSA). *Spectrochimica Acta*  
49 556 *Part A: Molecular and Biomolecular Spectroscopy*, 2014, 118, 48-54.  
50 557  
51 558 40. F. Faridbod, M.R. Ganjali, B. Larijani, S. Riahi, A.A. Saboury, M. Hosseini, ... & C.  
52 559 Pillip. Interaction study of pioglitazone with albumin by fluorescence spectroscopy and  
53 560 molecular docking. *Spectrochimica Acta Part A: Molecular and Biomolecular*  
54 561 *Spectroscopy*, 2011, 78(1), 96-101.  
55 562  
56 563 41. Y. Yue, Y. Wang, Q. Tu, Y. Xu, Y. Zhang, Q. Tang, J. Liu. A comprehensive insight  
57 564 into the effects of punicalagin on pepsin: Multispectroscopy and simulations  
58 565 methods. *Journal of Molecular Liquids*, 2022, 365, 120194.  
59 566  
60 567 42. F. Wong, A. Krishnan, E.J. Zheng, H. Stärk, A.L. Manson, A.M. Earl, ... & J.J. Collins.  
568 569 Benchmarking AlphaFold-enabled molecular docking predictions for antibiotic  
569 570 discovery. *Molecular systems biology*, 2022, 18(9), e11081.

- 1  
2  
3 557 43. Y. Wang, Y. Zhou, F.I. Khan. Molecular Insights into Structural Dynamics and Binding Interactions of Selected Inhibitors Targeting SARS-CoV-2 Main  
4 558 Protease. *International Journal of Molecular Sciences*, 2024, 25(24), 133482. View Article Online  
DOI: 10.1039/D3AY01534K
- 5 559  
6 560 44. W. Li, S. Huang, H. Wen, Y. Luo, J. Cheng, Z. Jia, ... & W. Xue. Pyridine  
7 561 functionalized carbon dots for specific detection of tryptophan in human serum samples  
8 562 and living cells. *Microchemical Journal*, 2020, 154, 104579.
- 9 563 45. S. Marincean, M. Al-Modhafir, D.B. Lawson.  $\pi$ - $\pi$  stacking interactions in tryptophan-  
10 564 lumiflavin-tyrosine: a structural model for riboflavin insertion into riboflavin-binding  
11 565 protein. *Journal of Molecular Modeling*, 2025, 31(2), 38.
- 12 566 46. D.A. Dougherty. Cation- $\pi$  interactions involving aromatic amino acids. *The Journal of*  
13 567 *nutrition*, 2007, 137(6), 1504S-1508S.
- 14 568 47. S. Dawn, P. Manna, T. Das, P. Kumar, M. Ray, S. Gayen, S.A. Amin. Exploring  
15 569 fingerprints for antidiabetic therapeutics related to peroxisome proliferator-activated  
16 570 receptor gamma (PPAR $\gamma$ ) modulators: A chemometric modeling approach.  
17 571 *Computational Biology and Chemistry*, 2024, 112, 108142.
- 18 572 48. S. Khatun, I. Dasgupta, S. Sen, S.A. Amin, I.A. Qureshi, T. Jha, S. Gayen. Histone  
19 573 deacetylase 8 in focus: Decoding structural prerequisites for innovative epigenetic  
20 574 intervention beyond hydroxamates. *International Journal of Biological*  
21 575 *Macromolecules*, 2025, 284, 138119.
- 22 576 49. A. Bhattacharjee, S. Kar, P.K. Ojha. Unveiling G-protein coupled receptor kinase-5  
23 577 inhibitors for chronic degenerative diseases: Multilayered prioritization employing  
24 578 explainable machine learning-driven multi-class QSAR, ligand-based pharmacophore  
25 579 and free energy-inspired molecular simulation. *International Journal of Biological*  
26 580 *Macromolecules*, 2024, 269, 131784.
- 27 581 50. S. Sharmeen, A. Woolfork, D.S. Hage. Generation of affinity maps for  
28 582 thiazolidinediones with human serum albumin using affinity microcolumns. I. Studies  
29 583 of effects by glycation on multisite drug binding. *Journal of Chromatography B*, 2024,  
30 584 1236, 124070.

### Data Availability Statement

View Article Online  
DOI: 10.1039/D5AY01534K

The authors confirm that the data supporting the findings of this study are available within the article [and/or] its supplementary materials.

Analytical Methods Accepted Manuscript

1  
2  
3  
4  
5  
6  
7  
8  
9  
10  
11  
12  
13  
14  
15  
16  
17  
18  
19  
20  
21  
22  
23  
24  
25  
26  
27  
28  
29  
30  
31  
32  
33  
34  
35  
36  
37  
38  
39  
40  
41  
42  
43  
44  
45  
46  
47  
48  
49  
50  
51  
52  
53  
54  
55  
56  
57  
58  
59  
60

Open Access Article. Published on 05 February 2026. Downloaded on 02/27/2026 4:34:43 AM.  
This article is licensed under a Creative Commons Attribution-NonCommercial 3.0 Unported Licence.  
